Bioactive Materials 16 (2022) 82–94

Contents lists available at ScienceDirect

Bioactive Materials

journal homepage: www.keaipublishing.com/en/journals/bioactive-materials

# Adoptive transfer of metabolically reprogrammed macrophages for atherosclerosis treatment in diabetic *ApoE*$^{-/-}$ mice

Tingting Wang [a,b,1], Yan Dong [c,1], Li Yao [d,1], Fan Lu [e,1], Chenxi Wen [b], Zhuo Wan [c], Li Fan [a,b], Zhelong Li [f], Te Bu [f], Mengying Wei [e,*], Xuekang Yang [b,**], Yi Zhang [a,***]

[a] Department of Equipment Division, School of Stomatology, Fourth Military Medical University, Xi'an, 710032, People's Republic of China
[b] Department of Burns and Cutaneous Surgery, Xijing Hospital, Fourth Military Medical University, Xi'an, 710032, People's Republic of China
[c] Department of Hematology, Tangdu Hospital, Fourth Military Medical University, Xi'an, 710038, People's Republic of China
[d] Department of Pathology, Xi'an No. 3 Hospital, The Affiliated Hospital of Northwest University, Xi'an, 710018, People's Republic of China
[e] Department of Biochemistry and Molecular Biology, Fourth Military Medical University, Xi'an, 710032, People's Republic of China
[f] Department of Ultrasound Diagnostics, Tangdu Hospital, Fourth Military Medical University, Xi'an, 710038, People's Republic of China

ARTICLE INFO

*Keywords:*
Atherosclerosis
Diabetes
Macrophage
*Acsl1*
Adoptive transfer

ABSTRACT

Atherosclerosis is characterized by inflammation in the arterial wall, which is known to be exacerbated by diabetes. Therapeutic repression of inflammation is a promising strategy for treating atherosclerosis. In this study, we showed that diabetes aggravated atherosclerosis in apolipoproteinE knockout (*ApoE*$^{-/-}$) mice, in which increased expression of long-chain acyl-CoA synthetase 1 (*Acsl1*) in macrophages played an important role. Knockdown of *Acsl1* in macrophages (M$\varphi^{shAcsl1}$) reprogrammed macrophages to an anti-inflammatory phenotype, especially under hyperglycemic conditions. Injection of M$\varphi^{shAcsl1}$ reprogrammed macrophages into streptozotocin (STZ)-induced diabetic *ApoE*$^{-/-}$ mice (*ApoE*$^{-/-}$+ STZ) alleviated inflammation locally in the plaque, liver and spleen. Consistent with the reduction in inflammation, plaques became smaller and more stable after the adoptive transfer of reprogrammed macrophages. Taken together, our findings indicate that increased *Acsl1* expression in macrophages play a key role in aggravated atherosclerosis of diabetic mice, possibly by promoting inflammation. Adoptive transfer of *Acsl1* silenced macrophages may serve as a potential therapeutic strategy for atherosclerosis.

## 1. Introduction

Atherosclerosis is a chronic inflammatory disease characterized by an imbalance in lipid metabolism and the accumulation of cholesterol-rich macrophages in the arterial wall [1,2]. Atherosclerosis is often prevalent in elderly people, many of whom are diabetic [3,4]. Notably, patients with diabetes have more severe atherosclerosis than patients without diabetes [5,6].

Diabetes mellitus causes greater inflammatory cell infiltration, macrophage and T lymphocyte migration, larger necrotic core formation, and more diffuse atherosclerosis in the coronary arteries, and ultimately accelerates atherosclerosis [7–9]. In mice, diabetes increases the number of monocytes by activating bone marrow precursors, leading to the infiltration of monocytes and increased macrophage numbers in plaques [10,11]. Diabetes mellitus promotes macrophage secretion of pro-inflammatory mediators, such as tumor necrosis factor (TNF)-α and interleukin (IL)-1β [12–14]. Moreover, hyperglycemia accelerates the transition of macrophage polarization from the alternative anti-inflammatory macrophage activation state to a classic pro-inflammatory macrophage activation state in diabetes [15,16].

Anti/proinflammatory macrophages exhibit important differences in metabolism. Anti-inflammatory macrophages depend more on fatty acid oxidation, whereas pro-inflammatory macrophages rely on a change in glycolysis [17]. Acyl coenzyme A synthetase-1 (ACSL1) promotes the

Peer review under responsibility of KeAi Communications Co., Ltd.
* Corresponding author.
** Corresponding author.
*** Corresponding author.
*E-mail addresses:* tonywei123@163.com (M. Wei), yangxuekangburns@163.com (X. Yang), zhangyi@fmmu.edu.cn (Y. Zhang).
[1] Contributed authors.

https://doi.org/10.1016/j.bioactmat.2022.02.002
Received 2 July 2021; Received in revised form 24 January 2022; Accepted 7 February 2022
Available online 15 February 2022

uptake of long-chain fatty acids and plays an important role in lipid metabolism [18,19]. Moreover, overexpression of *Acsl1* in macrophages leads to decreased expression of ABCA1, suggesting an important role of ACSL1 in cholesterol transport [20]. In contrast, the protective role of myeloid *Acsl1* deficiency has already been shown by transplanting bone marrow from mice with myeloid *Acsl1*-deficiency into virally induced $Ldlr^{-/-}$ mice [21,22].

In our study, we showed that diabetes aggravated atherosclerosis in $ApoE^{-/-}$ mice, mainly due to increased local and systemic inflammation. Moreover, increased expression of *Acsl1* in macrophages from diabetic mice is responsible for exacerbated inflammation. Injection of the reprogrammed macrophages into $ApoE^{-/-}$+ STZ mice alleviated both local inflammation in the plaque and systemic inflammation in the liver and spleen. Together, our findings indicate that increased *Acsl1* expression in macrophages is a key player in aggravated atherosclerosis, and adoptive transfer of *shAcsl1* lentivirus-infected macrophages is a potential therapeutic strategy for atherosclerosis treatment.

## 2. Materials and methods

### 2.1. Diabetic mouse model

Green fluorescent protein ($GFP^+$) transgenic mice (stock No: 003291) were obtained from the Jackson Laboratory, and $ApoE^{-/-}$ mice (C57BL background) were obtained from the Model Animal Research Center of Nanjing University. All experimental procedures involving animals were approved by the Institutional Animal Care and Use Committee of the Fourth Military Medical University. For the diet-induced obesity study, 8-week-old male $ApoE^{-/-}$ mice and C57BL/6 mice were fed a 45% high-fat diet (HFD) for 12 weeks. Mice were then injected with streptozotocin (STZ) (50 mg/kg, Sigma) or citrate buffer for five consecutive days to induce diabetes or serve as a control. After four weeks, blood glucose was assayed using the One Touch Ultra Blood Glucose Monitoring System (ACCU-CHEK Active, Roche 05144418).

### 2.2. Adoptive transfer of macrophages

$ApoE^{-/-}$ mice were fed with HFD. In the eighth week, diabetes was induced via STZ injection, as previously described. For prevention and therapy, the reprogrammed macrophages ($5 \times 10^6$ cells) were injected into $ApoE^{-/-}$+ STZ via the tail vein at weeks 6, 11, and 14, respectively. At the end of the experiments, mice were euthanized with pentobarbital sodium (100 mg/kg), and aortas and other tissues of interest were collected for further analysis.

### 2.3. Serum biochemistry

Mice were deeply anesthetized via intraperitoneal injection of pentobarbital sodium (100 mg/kg). Blood samples was drawn into BD Vacutainer Blood Collection Tubes ( BD, Bioscience) containing buffered sodium citrate as anticoagulant. Whole blood was placed at room temperature for 30 min and then centrifuged at 3000×*g* at 4 °C. After centrifugation, the serum was obtained for further analyses. The concentrations of alanine aminotransferase (ALT), aspartate aminotransferase (AST), plasma triglycerides, total cholesterol, high-density lipoprotein (HDL) cholesterol, and low-density lipoprotein (LDL) cholesterol were measured using Chemray 800 at Wuhan Servicebio Technology Co., Ltd.

### 2.4. Cell culture

The RAW264.7 cell line was obtained from ATCC. All cells were cultured in complete media containing high glucose Dulbecco's modified Eagle medium (DMEM) (Hyclone, USA) supplemented with 10% fetal bovine serum (FBS; Exocell, China) and 1% antibiotics (100 U/mL penicillin and 100 μg/mL streptomycin) from GIBCO at 37 °C with 5% $CO_2$.

### 2.5. Isolation and culture of bone marrow-derived macrophages (BMDMs)

Femurs and tibias from $GFP^+$ transgenic mice and $ApoE^{-/-}$ mice were harvested, and bone marrow was flushed using DMEM to collect bone marrow cells. After centrifugation, the cell pellet was resuspended in ACK lysis buffer (Sangon Biotech) for 5 min to remove red blood cells. Cells were then incubated in tissue plates at 37 °C in 5% $CO_2$ in the presence of M-CSF (20 ng/mL, Sino Biological Inc. Beijing) for six days in DMEM supplemented with 10% FBS and 1% antibiotics, with media being changed every two days. Anti-inflammatory macrophage or pro-inflammatory macrophage polarization was induced in cells using IL-4 (20 ng/mL, Peprotech, Rocky Hill, CT, USA) or IFN-γ (20 ng/mL, Peprotech Rocky Hill, CT) and lipopolysaccharide (LPS, 50 ng/mL, Sigma) in DMEM with 10% FBS for 12 h, respectively. To study the effects of glucose, macrophage differentiation and activation were performed in DMEM supplemented with either 5.5 (normal) or 25 mM (high) endotoxin-free D-glucose (Sigma Aldrich).

### 2.6. Virus infection and macrophage engineering

RAW264.7 cells or BMDMs were seeded into 6-well plates and incubated at 37 °C with 5% $CO_2$ overnight. RAW264.7 cells or macrophages were infected with *shAcsl*1 lentiviruses (Gene Pharma) at MOI = 10. The sequences targeting the control or *Acsl1* are listed in Table S1. The experimental procedure was conducted according to the manufacturer's instructions. Briefly, the cells were infected with lentivirus containing 8 μg of polybrene (Sigma, St. Louis, USA). Cells then received fresh medium after infection for 12 h.

### 2.7. Flow cytometry

To measure the effect of *shAcsl1* on the polarization of BMDMs, cells were exposed to vehicle or $1 \times 10^9$ TU/mL *shAcsl1* lentiviruses for three days. In some experiments, cells were treated with 5.5 (normal) or 25 mM (high) endotoxin-free D-glucose (Sigma Aldrich) before analysis. Briefly, cells were incubated with fluorescence-labeled antibodies (CD11b-APC, F4/80-Alexa Fluor 488, and CD86-PE or CD206-PE, Biolegend, USA) for 30 min. The cells were then washed three times with FACS buffer, followed by analysis using the BD FACS Calibur™. Flow cytometry data were analyzed using FlowJo software.

### 2.8. Macrophage trafficking

For *in vivo* tracking of macrophages in distribution analysis, BMDMs were obtained from C57BL/6-Tg (CAG-EGFP) 1Osb/J mice and treated with *shCtrl* and *shAcsl1* lentiviruses. Macrophages were injected into $ApoE^{-/-}$+ STZ mice via the tail vein. After 4 h or 72 h, $ApoE^{-/-}$+ STZ mice were anesthetized with pentobarbital sodium (50 mg/kg), and various organs were collected and stored in 4% paraformaldehyde (PFA; Thermo Fisher). For immunofluorescence staining, tissues were fixed in 4% PFA, mounted in paraffin blocks, and sectioned at 8 μm. Cell nuclei were counter-stained using Hoechst33342 (1:1000, Beyotime Biotechnology) for 15 min at room temperature in the dark. Images were captured using a laser scanning confocal microscope (Nikon A1R, Tokyo, Japan). We selected central veins as the origin and selected four quadrants. Each quadrant covered an area of 160,000 $\mu m^2$. The number of counted cells in more than 20 sections was averaged.

### 2.9. Histopathological staining and immunofluorescence analysis

Mice treated with the indicated treatments were euthanized with pentobarbital sodium (100 mg/kg). Tissues were fixed in 4% PFA, mounted in paraffin blocks, and sliced at 8 μm. Frozen aortic roots were

dissected for serial 8 μm cryo-sectioning that covered 500 μm of the root. Aortic root sections were stained with hematoxylin and eosin (H&E), Oil Red O (Sigma), Masson's trichrome staining (Solarbio, China), and anti-ACSL1 (Abcam, ab177958) antibodies. Furthermore, quantitative analysis of atherosclerotic plaques was performed using Image-Pro Plus 6.0. For immunofluorescence analysis, mice were sacrificed, and tissues of interest were dissected. Tissues were fixed in 4% PFA, mounted in paraffin blocks, and sliced into 8 μm sections. CD68+iNOS+ and CD68 + ARG1+ cells in aortic roots were double stained with corresponding antibodies: CD68 (Abcam, ab53444), iNOS (Abcam, ab178945), and ARG1 (Abcam, ab91279), followed by incubation with specific fluorescence-labeled secondary antibodies for 2 h. Cell nuclei were counter-stained with Hoechst33342 for 15 min at room temperature in the dark. Images were captured using a laser scanning confocal microscope (Nikon A1R, Tokyo, Japan).

### 2.10. RNA isolation and qRT-PCR

Total RNA from the cells and tissues was extracted using TRIzol (Invitrogen, USA) as per the instructions provided by the manufacturer, and mRNA was reverse transcribed using a transcribed First-strand cDNA Synthesis Kit (Roche), following the manufacturer's protocol. qPCR was performed using SYBR Green PCR Master Mix (Roche). Relative expression of mRNA was normalized to *GAPDH* and *β-actin* and calculated using the $2^{-\Delta\Delta Ct}$ method. The sequences of the PCR primers are listed in Supplementary Table 1.

### 2.11. Western blot analysis

Tissues and cells were harvested in 1 × RIPA buffer containing a protease inhibitor (Beijing, China). Samples were shaken on a rotator for 30 min and subsequently centrifuged at 12,000 rpm for 20 min at 4 °C. Protein concentration was determined using the Pierce BCA Protein Assay Kit (Thermo, USA). Protein samples were separated by sodium dodecyl sulphate-polyacrylamide gel electrophoresis (SDS-PAGE) and transferred to a nitrocellulose membrane in an ice bath. Membrane was blocked with 5% bovine serum albumin for 1 h and incubated overnight with primary antibodies at 4 °C. The antibodies used were rabbit anti-ACSL1 (Abcam, ab177958) and rabbit anti-GAPDH (Abcam, ab181602). Membranes were then incubated with the corresponding secondary antibodies for 1 h at room temperature. The bands were visualized using ECL Prime western blotting Detection Reagent (GE Healthcare, Buckinghamshire, UK).

### 2.12. Statistical analysis

All experimental data are presented as mean ± S.E.M. Student's *t*-test and one-way ANOVA were used to compare groups. Data were analyzed using GraphPad Prism 7 software. Statistical significance was set at $P < 0.05$.

## 3. Results

### 3.1. Diabetes exacerbates atherosclerosis in ApoE$^{-/-}$ mice

To induce atherosclerosis in diabetic mice, mice were fed a HFD for 12 weeks, then injected with streptozotocin to induce diabetes (Fig. 1A). Diabetic *ApoE*$^{-/-}$ (*ApoE*$^{-/-}$+ STZ) mice exhibited elevated blood glucose levels compared to C57, C57 + STZ, and *ApoE*$^{-/-}$ mice (Fig. 1B). In *ApoE*$^{-/-}$+ STZ mice, total cholesterol and LDL levels were higher than that observed in *ApoE*$^{-/-}$ mice (Fig. 1C, E). In contrast, no significant differences in triglyceride and HDL were found among C57, C57 + STZ, *ApoE*$^{-/-}$, and *ApoE*$^{-/-}$+ STZ mice (Fig. 1D, F). Atherosclerotic plaque formation results from chronic inflammation and fibroproliferative remodeling of the vascular wall. Notably, the C57 and C57 + STZ mice did not show plaque growth. Furthermore, Oil Red O staining of both aortic tree and roots demonstrated that the atherosclerotic plaque burden was much higher in *ApoE*$^{-/-}$+ STZ mice than in *ApoE*$^{-/-}$ mice (Fig. 1I, N, K, L, and Fig. S1B). Moreover, HE staining of the aortic root revealed that the necrotic core was much larger in *ApoE*$^{-/-}$+ STZ mice than in *ApoE*$^{-/-}$mice (Fig. 1G and J, and Fig. S1A). Plaque rupture is thought to be caused by the loss of mechanical stability, often due to the reduced tensile strength of the collagen cap surrounding the plaque [23]. Therefore, plaques with reduced collagen content are believed to be more vulnerable than those with thick collagen caps [24]. Notably, Masson's trichrome staining revealed reduced collagen content in the lesions of *ApoE*$^{-/-}$+ STZ mice compared to that in control *ApoE*$^{-/-}$ mice, suggesting that the plaque in the group may be unstable (Fig. 1H and M, Fig. S1C). Overall, these data indicated that diabetes exacerbates atherosclerosis in *ApoE*$^{-/-}$ mice.

### 3.2. Increased expression of Acsl1 in macrophages in mice

Diabetes accelerates the formation of atherosclerotic lesions by promoting macrophage accumulation in the susceptible arteries. To explore whether *Acsl1* may contribute to atherosclerosis in *ApoE*$^{-/-}$+ STZ mice. ACSL1 expression in C57, C57 + STZ, *ApoE*$^{-/-}$, and *ApoE*$^{-/-}$+ STZ mice were analyzed. *Acsl1* was highly expressed in macrophages from *ApoE*$^{-/-}$+ STZ mice compared to C57, C57 + STZ, and *ApoE*$^{-/-}$ mice. The level of *Acsl1* also increased in the ApoE control compared with the C57 control (Fig. 2A–D). In addition, we performed histochemistry analyses on atherosclerotic lesions using *Acsl1* antibodies. The results showed that *Acsl1* was highly expressed in the aortic root of *ApoE*$^{-/-}$+ STZ mice (Fig. S2A). Consistently, we also observed that *ApoE*$^{-/-}$+ STZ mice showed high expression of *Acsl1* in the aortic root (Figs. S2B–D).

Diabetes influences a wide spectrum of hepatic damage and often hastens the progression of steatosis through increased inflammation [25,26]. To directly evaluate the effects of diabetes-induced liver injury, histopathological observations of the liver were performed. As shown in Fig. S3A, liver tissues were intact, hepatic lobules were clear, and hepatocytes were regularly arranged in C57 mice. Only a slight increase in the number of inflammatory cells and swelling in liver cells was observed in C57 + STZ mice compared with that in C57 mice. In *ApoE*$^{-/-}$+ STZ mice, it was found that the basic architecture of liver cells disappeared, and apparent steatosis and liver cell swelling were observed, with increased infiltration of inflammatory cells compared with *ApoE*$^{-/-}$ mice. Furthermore, Masson's trichrome staining revealed significantly increased collagen content in *ApoE*$^{-/-}$+ STZ (Figs. S3B and G). To investigate whether hepatic damage is closely associated with the increased expression of *Acsl1* in the liver, we performed immunohistochemical analysis of the liver using *Acsl1* antibodies. Results showed that ACSL1 was highly expressed in *ApoE*$^{-/-}$+ STZ mice (Fig. S3C). Interestingly, *Acsl1* gene levels were also increased in *ApoE*$^{-/-}$+ STZ mice (Fig. S3F). We also observed that ACSL1 protein levels were increased in *ApoE*$^{-/-}$+ STZ mice (Figs. S3D–E). We measured the expression of inflammatory factors, including *Tnfa* (Fig. S3H), *Il-1β* (Fig. S3I), *Ptges* (Fig. S3J), and prostaglandin-endoperoxide synthase 2 (*Ptgs2*) (Fig. S3K), using qPCR. The results showed that inflammatory factors were increased in *ApoE*$^{-/-}$+ STZ mice, along with increased ACSL1 expression.

Myeloid progenitor cells develop into circulating monocytes, and the spleen acts as a reservoir for monocytes infiltrating atherosclerotic lesions [27,28]. Next, we evaluated diabetes-induced spleen injury by observing changes to spleen tissue. In C57 mice, lymphocytes were arranged neatly, and the boundary between the white and red pith was clear compared to the C57 + STZ mice. Further analysis of *ApoE*$^{-/-}$+ STZ mice revealed disorganization of lymphocytes and a blurring of boundaries between the white and red pith compared with *ApoE*$^{-/-}$ mice (Fig. S4A). Consistently, we also observed that *ApoE*$^{-/-}$+ STZ mice displayed increased *Acsl1* expression in the spleen (Figs. S4B–E). Furthermore, we extracted mRNA from the spleen tissue and observed an

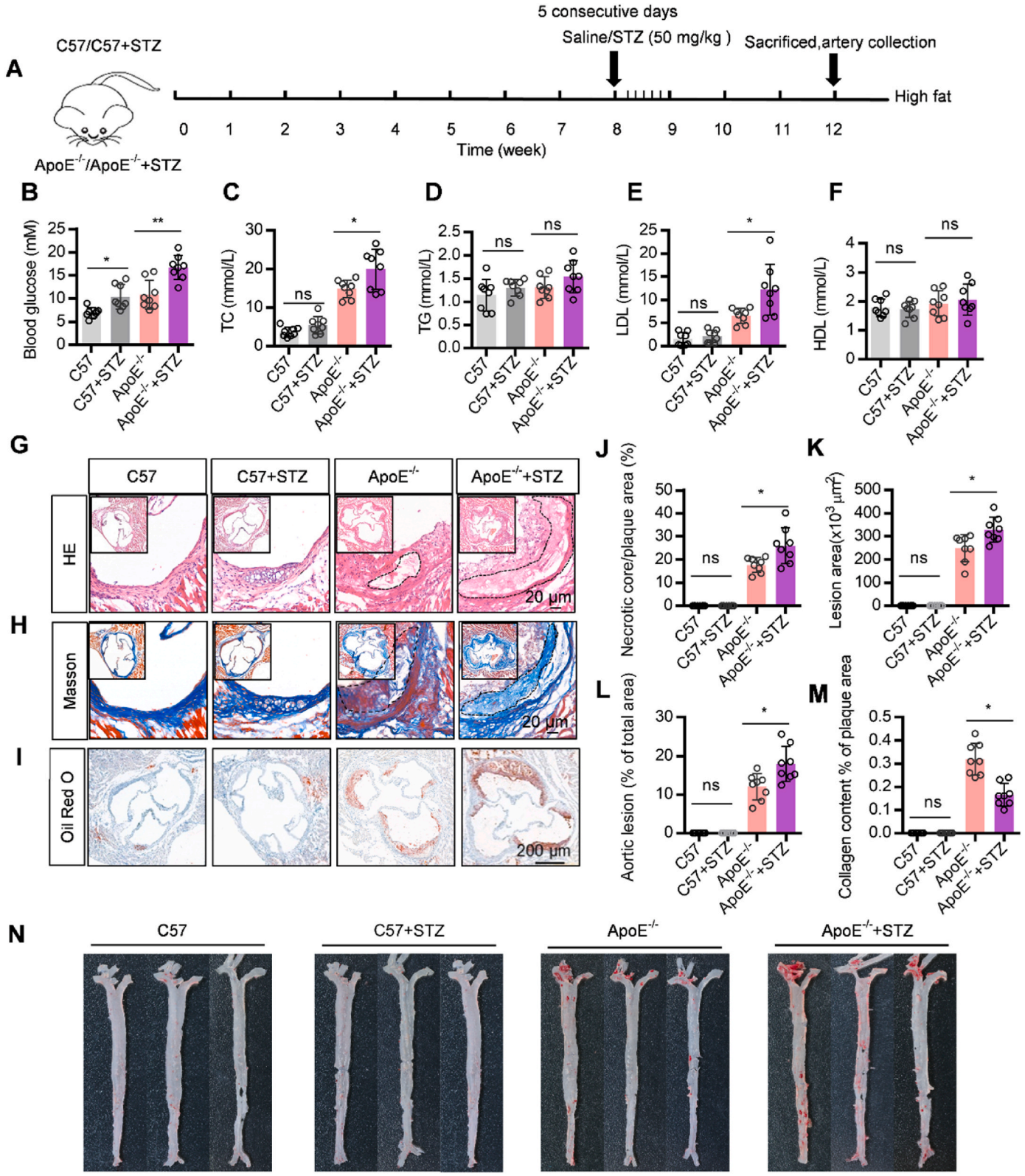


**Fig. 1. Diabetes accelerates atherosclerosis in *ApoE*$^{-/-}$ mice.** A. A schematic diagram showing the experimental procedure. Apolipoprotein knockout (*ApoE*$^{-/-}$) mice were fed a 45% high -fat diet (HFD) for 12 weeks and injected with streptozotocin (STZ) for five consecutive days during the eighth week to induce diabetes. B. Blood glucose levels measured in mice. C–F. Examination of the total cholesterol (C), total triglyceride (D), low-density lipoprotein (LDL) (E), and high-density lipoprotein (HDL) (F) levels. G–I. Representative images of the atherogenic lesion areas stained with hematoxylin and eosin (H&E) (G), Masson's trichrome (H), and Oil Red O (I). Scale bar = 20 or 200 μm. J–K. Quantitative analysis of the necrotic core area, lesion areas relative to plaque area from G and H. L. Percentage analysis of the atherosclerosis region from N. M. Quantitative analysis of plaque collagen area relative to plaque area from H. All data are expressed as mean ± SD (n = 8 per group). $^{*}P < 0.05$ and $^{**}P < 0.01$, using one-way ANOVA; ns, no significance. (For interpretation of the references to colour in this figure legend, the reader is referred to the Web version of this article.)

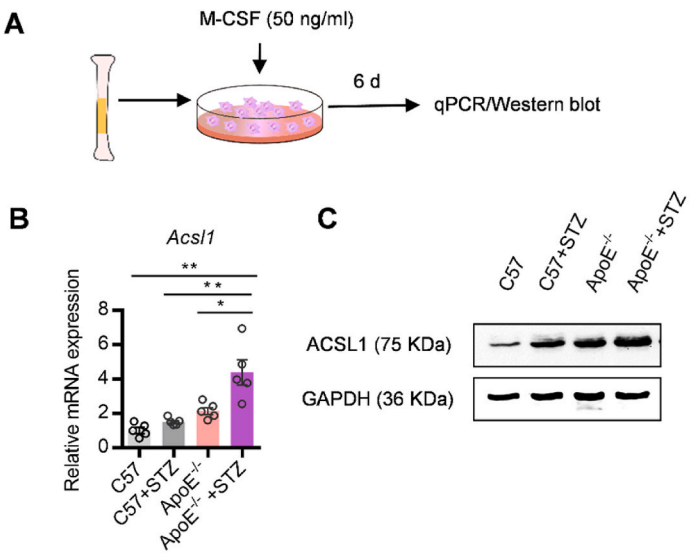


**Fig. 2. Increased expression of Acyl coenzyme A synthetase-1 (*Acsl1*) in macrophages from mice.** A. Experimental procedure. Mice were sacrificed, bone marrow was harvested, and macrophages were cultured. B. qPCR analysis of the expression of *Acsl1* mRNA in macrophages from mice as indicated. *Gapdh* served as an internal control. C. Western blot analysis of ACSL1 expression at the protein level in macrophages. GAPDH served as a loading control. D. Quantitative analysis of the western blot band density. All data are expressed as mean ± S.E.M of five independent experiments. $^{*}P < 0.05$, $^{**}P < 0.01$ using one-way ANOVA.

increase in inflammatory mediators in *ApoE*$^{-/-}$+ STZ mice (Figs. S4F–I). In summary, diabetes induces inflammatory changes in the mouse liver and spleen, which are associated with an increase in *Acsl1* in macrophages.

### 3.3. *Acsl1* knockdown induces anti-inflammatory macrophages

Our data demonstrated that *Acsl1* plays a key role in promoting inflammation in diabetes-accelerated atherosclerosis. Therefore, we

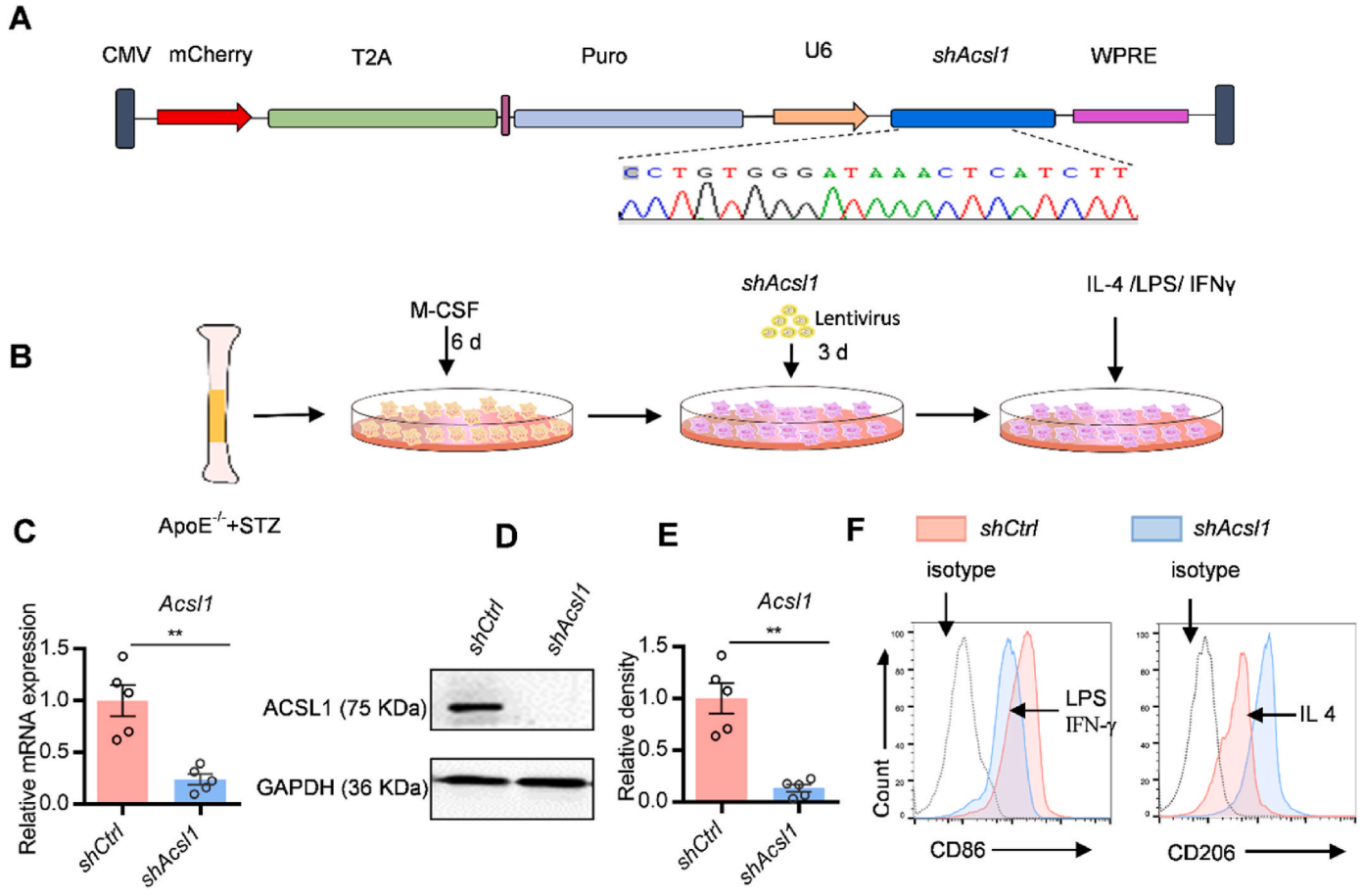


**Fig. 3. Knockdown of Acyl coenzyme A synthetase-1 (*Acsl1*) induces anti-inflammatory macrophage polarization.** A. Illustration of *Acsl1* gene silencing strategy. B. For the transfection experiment, shRNA-mediated *Acsl1* gene transfection of macrophages was conducted for 72 h. C. RNA expression of *Acsl1* in macrophages from *ApoE*$^{-/-}$+ STZ mice. *Gapdh* served as an internal control. D. Western blot analysis of ACSL1 at the protein level in macrophages from apolipoprotein knockout (*ApoE*$^{-/-}$) + streptozotocin (STZ) mice, GAPDH served as a loading control. E. Quantitative analysis of the western blot band density. F. Representative flow cytometry analysis for CD86/CD206 in macrophages differentiated with LPS, IFNγ, or IL4.

performed shRNA-mediated *Acsl1* gene silencing in RAW 264.7 cells and found that the infection efficiency was approximately 30–40% (Fig. S5A). We then isolated macrophages from *ApoE*$^{-/-}$+ STZ mice, performed shRNA-mediated *Acsl1* gene silencing on the macrophages and observed a decrease in *Acsl1* expression (Fig. 3A–E). These data indicate that the expression of *Acsl1* in macrophages can be efficiently and persistently repressed. To evaluate whether shRNA-mediated *Acsl1* gene silencing can induce macrophage polarization, the results showed that significantly increased the levels of several anti-inflammatory macrophage marker genes and induced significant mRNA changes in pro-inflammatory macrophage marker gene expression (Figs. S5B–C). In addition, *Acsl1* knockdown increased the number of anti-inflammatory macrophages, as suggested by flow cytometry analysis of CD86 (a pro-inflammatory macrophage marker) and CD206 (an anti-inflammatory macrophage marker) (Fig. 3F). Taken together, these data show that shRNA mediated *Acsl1* gene silencing can induce anti-macrophage polarization.

Hyperglycemia skews plaque macrophages towards an atherogenic proinflammatory phenotype instead of towards the atherosclerosis-resolving anti-inflammatory state [8]. We explored the potential function of *Acsl1* knockdown under high-glucose conditions. Flow cytometry analysis further confirmed an increase in anti-inflammatory macrophages in the *shAcsl1* group under high-glucose and low-glucose conditions (Fig. 4A–C). Interestingly, knockdown of *Acsl1* in macrophages resulted in an anti-inflammatory phenotype, even under hyperglycemic conditions. (Fig. 4D–O, Fig. S5E–P).

ACSL1 is reported to localize both in mitochondria and endoplasmic reticulum [29]. When generated in the mitochondrial outer membrane by ACSL1, acyl-CoAs are destined for β-oxidation. Although the fate of acyl-CoA produced by ER-localized ACSL1 is not clearly understood, it is likely involved in lipid synthesis, since the other key lipid synthetic enzymes (GPAT and DGAT) are localized in ER [30,31]. We explored a correlation between lipid metabolism and *Acsl1* in macrophages by analyzing its effects on accumulation of intracellular lipids in macrophages. The results showed that knocking down *Acsl1* in macrophages decreased the intracellular lipid droplet accumulation under hyperglycemic conditions (Figs. S6A–B). These data indicated ACSL1 reduction in macrophage reduced lipid accumulation under hyperglycemic condition.

Increased release of PGE2 has been reported previously in several cell types in response to diabetes or elevated glucose concentrations [32], and it has been shown to be caused by increased activity of calcium-dependent phospholipase A2, which catalyzes the release of arachidonic acid from membrane phospholipids [33]. We thus analyzed mRNA levels of enzymes in the PGE2 synthesis pathway. Knockdown of *Acsl1* reduced *Ptgs2* mRNA levels in pro-inflammatory macrophages (Fig. 4J). Similar results were obtained for microsomal *Ptges* mRNA (Fig. 4K). Thus, it is reasonable to deduce that knockdown of *Acsl1* in macrophages may regulate the inflammation at least partially via lipid metabolism regulation under hyperglycemic conditions.

### 3.4. Adoptive transfer of shAcsl1 reprogrammed macrophages alleviates atherosclerosis in diabetic ApoE$^{-/-}$ mice

Anti-inflammatory macrophage polarization may provide a promising strategy for atherosclerosis treatment in diabetes. We systematically analyzed the therapeutic effects of M$\varphi^{shAcsl1}$. For *in vivo* tracking, macrophages obtained from GFP $^{+}$ mice were injected into *ApoE*$^{-/-}$+ STZ mice via the tail vein. The results showed that more M$\varphi^{shAcsl1}$ was located in atherosclerosis plaque, liver, and spleen at 4 h in comparison with M$\varphi^{shCtrl}$ 72 h post-injection. (Fig. 5A–E, Fig. 7A–I). For treatment, approximately 5 × 10$^6$ reprogrammed macrophages were injected into diabetic *ApoE*$^{-/-}$ mice twice in one month (Fig. 6A). Blood glucose and lipid profiles did not significantly change in phosphate-buffered saline (PBS) mice compared to M$\varphi^{shAcsl1}$ mice (Fig. 6B–E). HDL-C significantly increased in M$\varphi^{shAcsl1}$ mice compared to M$\varphi^{shCtrl}$ mice (Fig. 6F), suggesting that any treatment effects are lipid-independent. Furthermore, histological analysis of the aortic tree and roots demonstrated that the atherosclerotic plaque was significantly attenuated in mice receiving M$\varphi^{shAcsl1}$ treatment (Fig. 6G–N and Figs. S7A–B). Notably, Masson's trichrome staining revealed that the collagen content in the plaque region also increased, suggesting that the plaque might become stable in the lesions of M$\varphi^{shAcsl1}$ mice (Fig. 6I, M and Fig. S7C). As mentioned previously, regressing plaques have reduced macrophage content, but have also shown a prevalence of both anti- and pro-inflammatory macrophages. iNOS and arginase 1 are commonly used as markers of pro-inflammatory macrophages and anti-inflammatory macrophages, respectively [34,35]. Thus, we evaluated the anti-inflammatory macrophage content in plaques and found that M$\varphi^{shAcsl1}$ treatment promoted the presence of anti-inflammatory macrophages over pro-inflammatory macrophages (Figs. S7D–E). Taken together, these data indicate that adoptive transfer of sh*Acsl1* reprogrammed macrophages alleviates atherosclerosis in diabetic *ApoE*$^{-/-}$ mice.

### 3.5. Adoptive transfer of reprogrammed macrophages reduced systemic inflammation in diabetic ApoE$^{-/-}$ mice

We further investigated the mechanism responsible for the *in vivo* treatment of atherosclerosis in these macrophages. First, we found that a higher number of GFP $^{+}$ macrophages were located in the liver and spleen 4 h after injection in comparison with M$\varphi^{shCtrl}$. After 72 h of injection, GFP$^{+}$ macrophages still appeared in the liver and spleen (Fig. 7A–I). For treatment, approximately 5 × 10$^6$ reprogrammed macrophages were injected into diabetic *ApoE*$^{-/-}$ mice twice in one month (Fig. 6A). In the PBS, Mφ, and M$\varphi^{shCtrl}$ mice, it was found that the basic architecture of the liver cells disappeared (Fig. 8A). In contrast, liver tissues were intact, hepatic lobules were clear, and hepatocytes were regularly arranged after M$\varphi^{shAcsl1}$ treatment. M$\varphi^{shAcsl1}$ treatment significantly reduced the accumulation of lipid droplets in hepatocytes (Figs. S8B and D). Masson's trichrome staining further confirmed that M$\varphi^{shAcsl1}$ treatment significantly reduced collagen content (Figs. S8A and C). We next assessed the effect of M$\varphi^{shAcsl1}$ treatment on liver function and observed that levels of serum biomarkers AST and ALT were significantly decreased in the M$\varphi^{shAcsl1}$ group (Fig. 8C and D). Moreover, qPCR analysis revealed that M$\varphi^{shAcsl1}$ treatment significantly reduced the expression of inflammatory genes (Fig. 8E–H). These data indicated that M$\varphi^{shAcsl1}$ treatment significantly decreased inflammation in the liver.

In the spleen, we observed disorganization of lymphocytes and a blurring of boundaries between the white and red pith in mice receiving PBS, Mφ, and M$\varphi^{shCtrl}$ treatments. In contrast, the lymphocytes were well arranged, and the boundary between the white and red pith was clear after M$\varphi^{shAcsl1}$ treatment. (Fig. 8B). Moreover, qPCR analysis revealed that M$\varphi^{shAcsl1}$ treatment significantly reduced the expression of inflammatory genes in the spleen (Fig. 8I–L). In summary, these data showed that adoptive transfer of reprogrammed macrophages reduces systemic inflammation in diabetic *ApoE*$^{-/-}$ mice. In addition, we further tracked macrophage distribution in other organs, and the results showed that GFP$^{+}$ macrophages rarely appeared in the kidney, lung, and heart at either 4 h or 72 h post-injection (Figs. S9A–E, S10A– E). These data indicate that adoptive transfer of reprogrammed macrophages did not cause any noticeable toxic effects in these organs.

## 4. Discussion

In our study, we confirmed for the first time that increased expression of *Acsl1* in macrophages is responsible for aggravated inflammation, and thus, exacerbated atherosclerosis. Knockdown of *Acsl1* in macrophages reprograms the cells to an anti-inflammatory phenotype. Adoptive transfer of reprogrammed macrophages significantly repressed inflammation and alleviated atherosclerosis in diabetic *ApoE*$^{-/-}$ mice.

Significant advances in therapies to prevent and/or treat

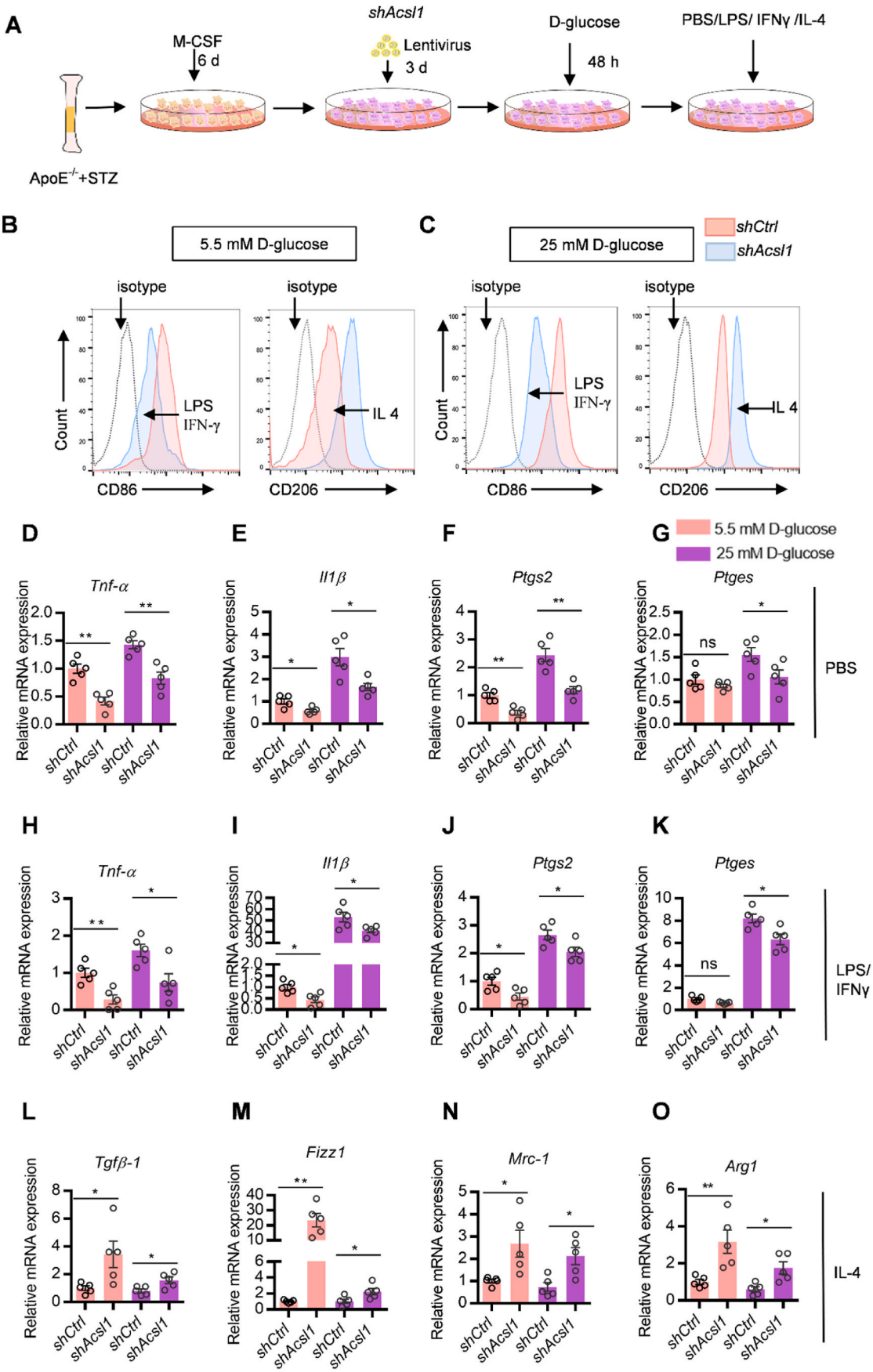


(caption on next page)

**Fig. 4. Knockdown of Acyl coenzyme A synthetase-1 (*Acsl1*) reduces inflammatory cytokine secretion in macrophages under high-glucose conditions.** A. Schematic diagram of the experimental procedure. Macrophages were differentiated with lipopolysaccharides (LPS), IFNγ, or IL4 in 5.5 (normal) or 25 mM (high) endotoxin-free D-glucose, respectively. B–C. Bone marrow-derived macrophages (BMDMs) were stained using CD86/CD206 and analyzed using flow cytometry. D–G. Expression of inflammatory genes *(Tnf-α, Il1β, Ptgs2, Ptges)* in macrophages treated with *shctrl* or *shAcsl1*. H–K. Expression of inflammatory cytokines *(Tnf-α, Il1β, Ptgs2, Ptges)* in BMDMs additionally treated with LPS. L–O. Expression of anti-inflammatory genes (*Tgfβ-1, Arg1, Fizz 1, Mrc1*) in macrophages additionally treated with IL-4. *Gapdh* served as an internal control. Data are expressed as mean ± S.E.M of five parallel experiments. $^{*}P < 0.05$, $^{**}P < 0.01$ using one-way ANOVA. ns, no significance.

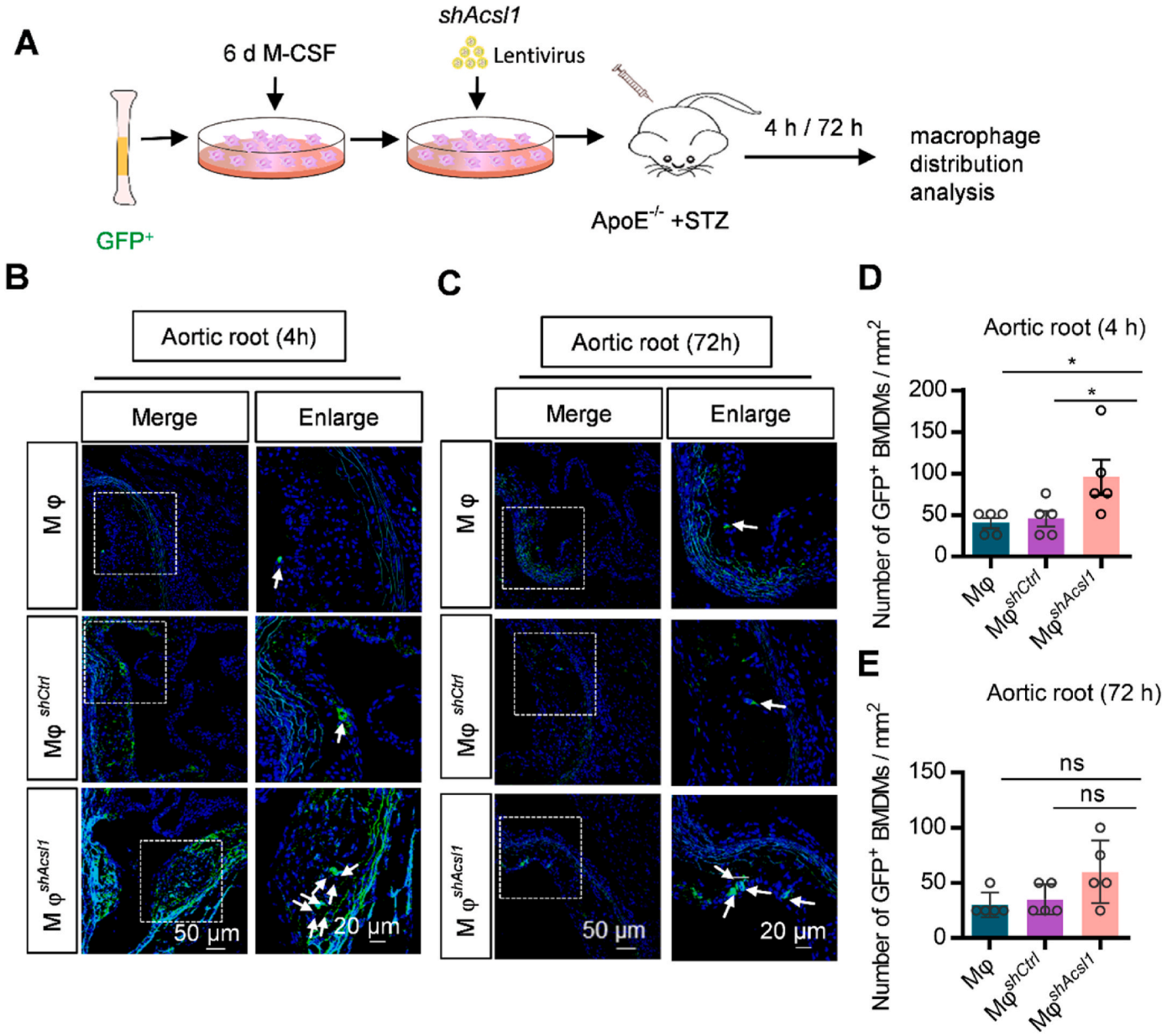


**Fig. 5. Distribution of injected macrophages in (*ApoE*$^{-/-}$) + streptozotocin (STZ) mice within 4 h or 72 h.** A. A schematic representation of the experimental procedure. Green fluorescent protein (GFP$^{+}$) macrophages were injected into *ApoE*$^{-/-}$+ STZ mice for tracking 4 h or 72 h post-injection. B–C. Representative fluorescence images of the GFP$^{+}$-labeled macrophages in the aorta root (green). The nuclei were counter-stained with Hoechst (blue). Scale bar = 50 or 20 μm (n = 5 per group). D–E. Quantitative analysis of the number of GFP$^{+}$ bone marrow-derived macrophages (BMDMs) per mm$^2$. (For interpretation of the references to colour in this figure legend, the reader is referred to the Web version of this article.)

atherosclerosis have been achieved in clinics [36,37]. For example, PCSK9 inhibitors lower plasma LDL-C levels and reduce the risk of major vascular events [38,39]. Patients with diabetes mellitus remain at an increased risk of cardiovascular morbidity and mortality [40,41]. Novel therapeutic strategies are urgently needed. Although it is believed that lesions of atherosclerosis from people with and without diabetes have no distinguishing morphological features, several mouse studies have suggested that there should be specific molecules involved in the mechanism how diabetes accelerated atherosclerosis. And ACSL1 might be such a candidate. In this study, we found that ACSL1 is expressed at higher levels in myeloid cells in mice with diabetes induced by STZ or virus [21,22]. Our results showed that ACSL1 was highly expressed in

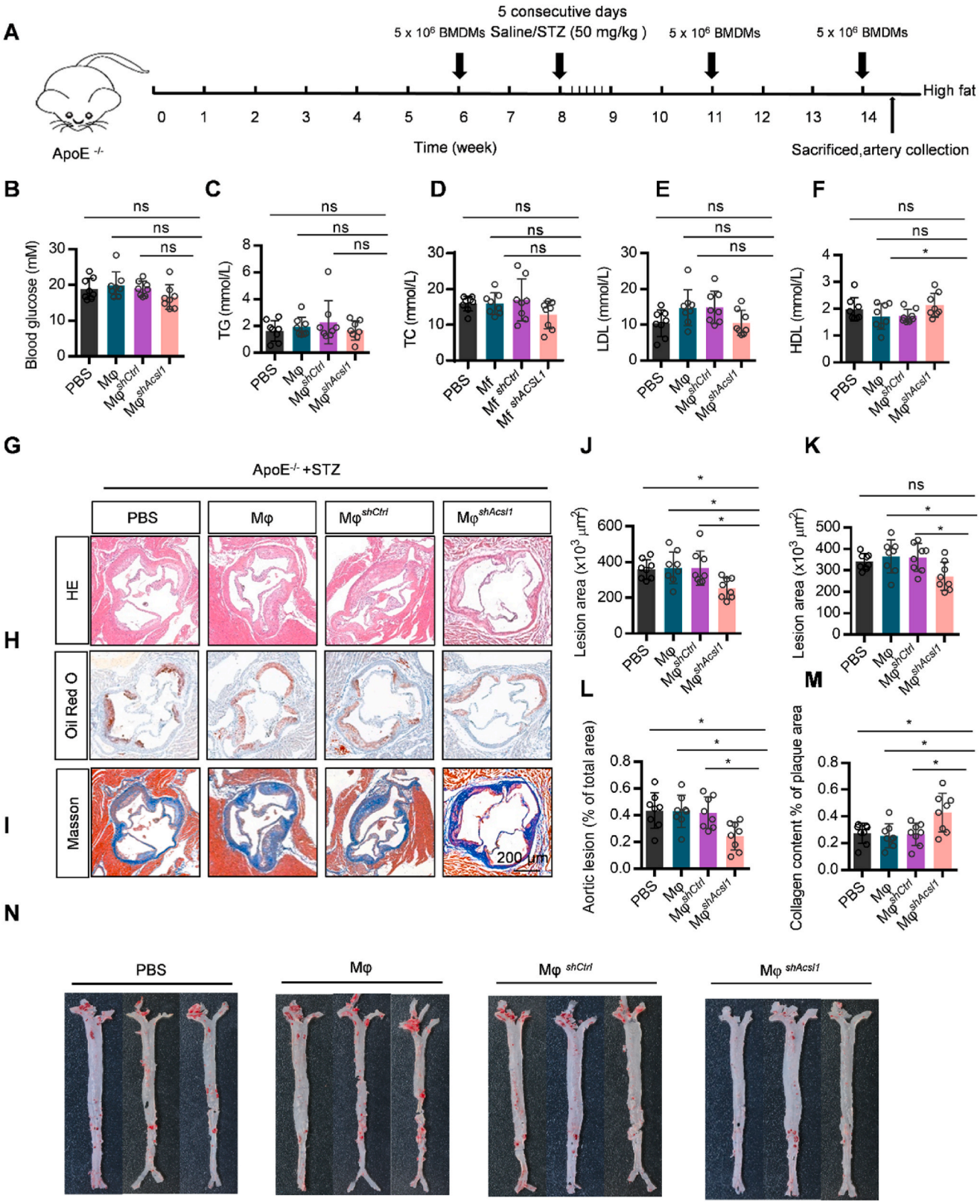


**Fig. 6. Therapeutic effects of Mφ$^{shAcsl1}$ in diabetic (*ApoE*$^{-/-}$) + streptozotocin (STZ) mice.** A. Schematic showing the experimental procedure. For the prevention and therapy, the reprogrammed macrophages ($5 \times 10^6$ cells) were injected into *ApoE*$^{-/-}$+ STZ mice via the tail vein at weeks 6, 11, and 14, respectively. B. Blood glucose level test results in mice. C–F. Examination of total triglyceride (C), total cholesterol (D), low-density lipoproteins (LDL) (E), and high-density lipoproteins (HDL) (F) levels. G–I. Representative images of the atherogenic lesion areas stained with hematoxylin and eosin (H&E) (G), Oil Red O (H), and Masson's trichrome (I). Scale bar = 200 μm. J–K. Quantitative analysis of the lesion areas relative to plaque area from G, H. L. Percentage analysis of the atherosclerosis region from N. M. Quantitative analysis of plaque collagen area relative to plaque area from I. Scale bar = 200 μm. All data are expressed as mean ± SD (n = 8 per group). *$P < 0.05$ using one-way ANOVA. ns, no significance. (For interpretation of the references to colour in this figure legend, the reader is referred to the Web version of this article.)

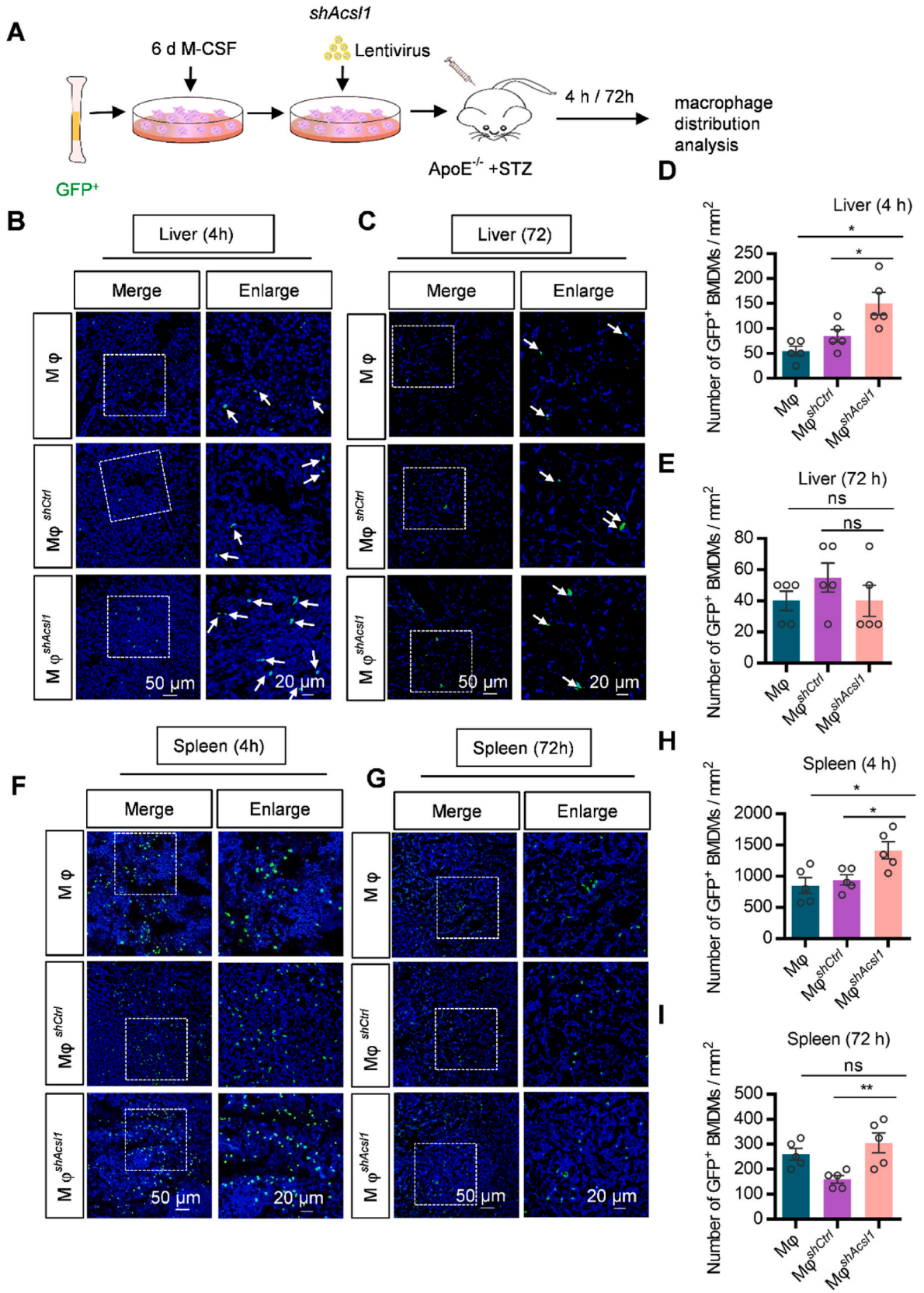


**Fig. 7. Distribution of macrophages in (*ApoE*$^{-/-}$-) + streptozotocin (STZ) mice within 4 h or 72 h.** A. Schematic representation of the procedure. Green fluorescent protein (GFP$^{+}$) macrophages were injected into *ApoE*$^{-/-}$+ STZ mice to enable tracking 4 h after injection. B–G. Representative fluorescence images of the GFP$^{+}$-labeled macrophages in the liver and spleen (green). The nuclei were counter-stained with Hoechst (blue). Scale bar = 50 or 20 μm (n = 5 per group). D–I. Quantitative analysis of the number of GFP$^{+}$ bone marrow-derived macrophages (BMDMs) per mm$^{2}$. (For interpretation of the references to colour in this figure legend, the reader is referred to the Web version of this article.)

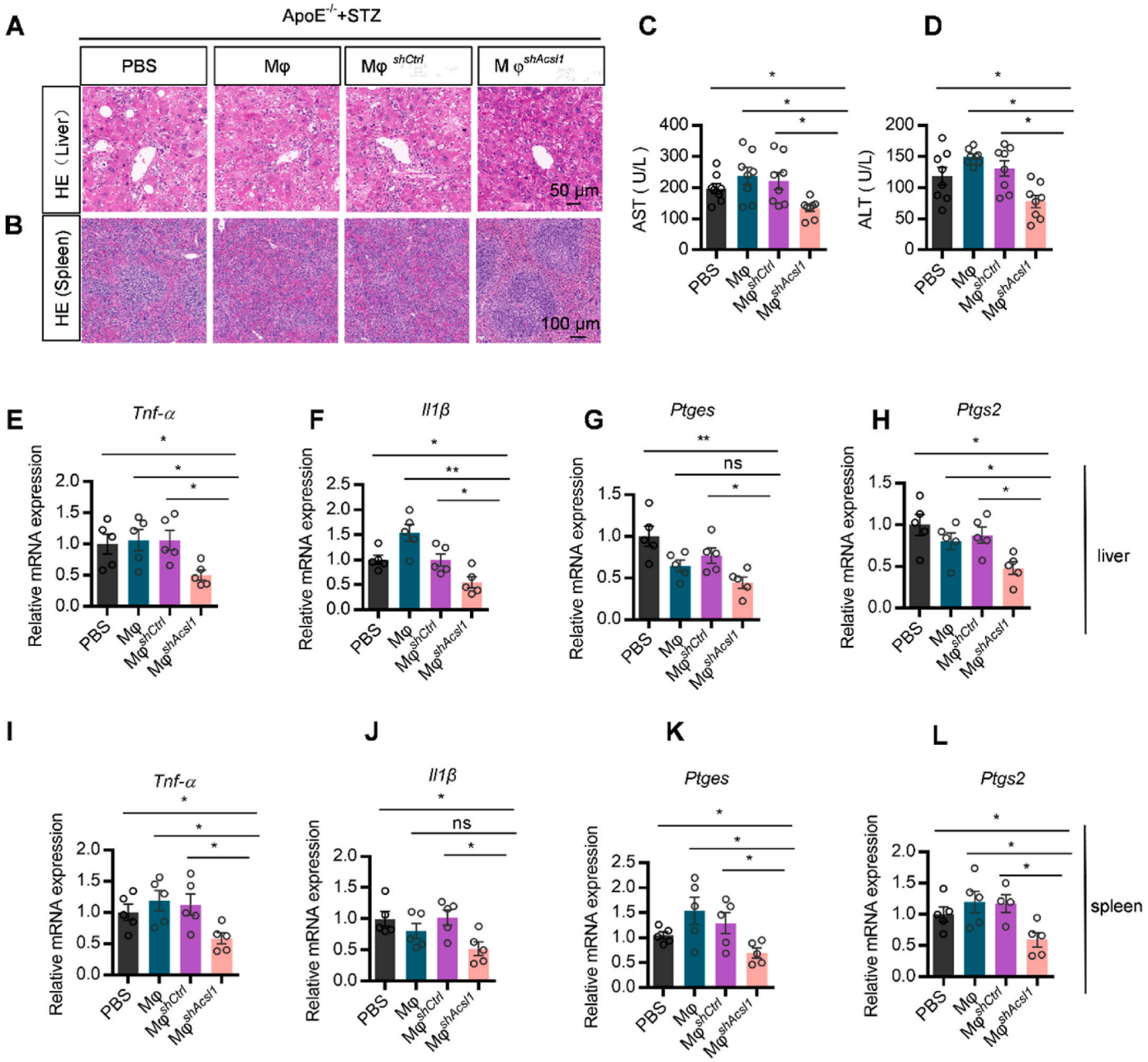


**Fig. 8. Adoptive transfer of reprogrammed macrophages alleviates inflammation in the liver and spleen of diabetic (*ApoE*$^{-/-}$) mice.** A. Schematic diagram of the experimental procedure. For the prevention and therapy, the reprogrammed macrophages ($5 \times 10^6$ cells) were injected into *ApoE*$^{-/-}$+ streptozotocin (STZ) mice via the tail vein at weeks 6, 11, and 14, respectively. A-B. Histology analysis of macrophages to treat liver and spleen. Scale bar = 50 or 100 μm. C–D. Plasma alanine transaminase (ALT) and aspartate transaminase (AST) levels (n = 8 per group). E–L. Expression of inflammatory genes (*Tnfα, Il1β, Ptges, Ptgs2*) in the liver and spleen of indicated mice. All data were expressed as mean ± S.E.M of five independent experiments. *$P < 0.05$ using one-way ANOVA. *Gapdh* served as an internal control.

monocytes of bone marrow, liver, and spleen of diabetic *ApoE−/−* mice. In addition, ACSL1 is localized in mitochondria, lipid droplets, endoplasmic reticulum and microsomes of liver [29,42,43]. Notably, ACSL1 is highly expressed by all parenchymal cells in ApoE$^{-/-}$ + STZ mice. The key function of ACSL1 in the liver remains to be explored.

A dominant hypothesis in atherosclerosis is that excessive inflammation or failed inflammation resolution is a major contributor to plaque development and late-stage lesion destabilization [23]. Despite a growth in understanding the chronic inflammatory nature of atherosclerosis, a specific anti-inflammatory therapy is yet to be found. It has been revealed that *Acsl1* induces the conversion of macrophages to the pro-inflammatory macrophage phenotype under diabetic conditions [44,45]. Another result provided evidence that TNF*α*-related inflammatory polarization in monocytes is an *Acsl1*-dependent process [46]. Furthermore, the aging macrophage significantly increases $PGE_2$ expression [47]. Our data showed that ACSL1 deficiency inhibited the release of inflammatory factors, *Ptges* and *Ptgs2,* by macrophages even in hyperglycemic condition.

Atherosclerosis is a localized and systemic metabolic inflammatory disease [48]. It has become clear that diabetes-induced chronic tissue inflammation, particularly in the liver and spleen, can cause atherosclerosis [49,50]. The liver is a major organ that regulates whole-body cholesterol metabolism. Disrupted hepatic cholesterol hemostasis contributes to atherogenesis [51]. Hepatic macrophages have a central role

in restricting inflammation in the liver [52]. Thus, targeting hepatic macrophages to treat liver disease may provide a potential therapeutic strategy [53]. The spleen also serves as a critical reservoir of monocytes that regulate inflammation during ischemic myocardial injury [54,55]. Due to the bone marrow origin of these monocytes, it has been recently recognized that splenic hematopoietic stem and progenitor cells can be an extramedullary myelopoietic source of monocytes that are mobilized to inflammatory sites, including atherosclerotic plaques [56]. Splenectomy accelerates atherogenesis by modulating lipid changes, implying a protective effect of the spleen [57,58]. Considering that macrophages serve as a bridge between liver, spleen and arteriosclerosis, we engineered macrophages. As expected, adoptive transfer of the reprogrammed macrophages in diabetic *ApoE*$^{-/-}$ mice alleviated inflammation locally in the plaque and systemically in the liver and spleen.

Macrophages are the central cells in atherosclerosis, and the quantity and phenotype of these cells in plaques influence both disease progression and regression [59–62]. With these factors, bone marrow macrophage therapy has shown promising results as a novel therapeutic approach for atherosclerosis that complements existing therapies. For example, studies have shown that soluble ninjurin [60], deletion of macrophage LRP1 [63], and RIPK1 antisense oligonucleotides [59] are intensively studied strategies for the treatment of atherosclerosis. Recently, adoptive macrophage transfer has shown promising results an effective therapeutic option for bacterial sepsis [64], liver fibrosis [65], ovarian cancer [66], and high-grade gliomas [67]. Furthermore, studies have demonstrated that injection of exogenous reprogrammed macrophages hijacks existing macrophages, recruits signals, and activates the immune system to destroy the tumor [68,69]. Macrophages represent a readily available, autologous source of cells for cell therapy. Moreover, the major advantage of macrophage therapy is that there is no need for long-term immune suppression to preserve the transplanted cells. Our study further confirmed that adoptive transfer of reprogrammed macrophages significantly alleviated atherosclerosis in diabetic *ApoE*$^{-/-}$ mice. At the same time, macrophages are safe to treat patients, and there are no adverse clinical reactions during infusion or in the post-infusion period [70].

Regarding the engineering strategy, we used shRNA mediated *Acsl1* gene silencing in BMDMs to induce anti-macrophages. There were more M$\varphi^{shAcsl1}$ in the liver and spleen, which could be attributed to altered viability or migration ability [71]. The reasons for this need to be explored further. Moreover, specifically engineered macrophages may have the ability to enter a lesion and migrate out of the damaged area. These potential treatment avenues need to be studied further.

## 5. Conclusion

In conclusion, our study provides evidence that increased expression of *Acsl1* in macrophages of diabetic mice play a key role in aggravated atherosclerosis of diabetic mice, possibly by promoting inflammation. Adoptive transfer of *Acsl1* silenced macrophages is a potential therapeutic strategy for atherosclerosis in patients with diabetes.

## CRediT authorship contribution statement

**Tingting Wang:** Writing – original draft, Writing – review & editing, Conceptualization, Investigation, Visualization. **Yan Dong:** Writing – review & editing, Methodology. **Li Yao:** Writing – review & editing, Methodology. **Fan Lu:** Resources, Data curation. **Chenxi Wen:** Investigation. **Zhuo Wan:** Investigation. **Li Fan:** Investigation. **Zhelong Li:** Validation, Formal analysis, Data curation. **Te Bu:** Investigation. **Mengying Wei:** Investigation, Data curation. **Xuekang Yang:** Supervision, Funding acquisition. **Yi Zhang:** Supervision, Funding acquisition, Project administration.

## Declaration of competing interest

The authors declare that they have no known competing financial interests or personal relationships that could have appeared to influence the work reported in this paper.

## Acknowledgements

The authors are grateful to Dailing Si for her assistance with the Nikon microscope system. This work was funded by the National Natural Science Foundation of China (No, 81671910 to X Yang ), Shanxi Province Foundation of China (No. 2021SF-341 to X Yang).

## Appendix A. Supplementary data

Supplementary data to this article can be found online at https://doi.org/10.1016/j.bioactmat.2022.02.002.

## References

[1] I. Tabas, K.E. Bornfeldt, Macrophage phenotype and function in different stages of atherosclerosis, Circ. Res. 118 (2016) 653–667, https://doi.org/10.1161/circresaha.115.306256.
[2] C. Lorenzo, et al., ALDH4A1 is an atherosclerosis auto-antigen targeted by protective antibodies, Nature 589 (2021) 287–292, https://doi.org/10.1038/s41586-020-2993-2.
[3] B.C. Jaeger, et al., Cardiovascular disease and mortality in adults aged ≥60 Years according to recommendations by the American college of cardiology/American heart association and American college of physicians/American academy of family physicians, Hypertension 73 (2019) 327–334, https://doi.org/10.1161/hypertensionaha.118.12291.
[4] A. Menke, S. Casagrande, L. Geiss, C.C. Cowie, Prevalence of and trends in diabetes among adults in the United States, 1988-2012, JAMA 314 (2015) 1021–1029, https://doi.org/10.1001/jama.2015.10029.
[5] R. Virmani, A.P. Burke, F. Kolodgie, Morphological characteristics of coronary atherosclerosis in diabetes mellitus, Can. J. Cardiol. 22 (Suppl B) (2006) 81b–84b, https://doi.org/10.1016/s0828-282x(06)70991-6.
[6] C.P. Cannon, et al., Cardiovascular outcomes with ertugliflozin in type 2 diabetes, N. Engl. J. Med. 383 (2020) 1425–1435, https://doi.org/10.1056/NEJMoa2004967.
[7] M.S. Shah, M. Brownlee, Molecular and cellular mechanisms of cardiovascular disorders in diabetes, Circ. Res. 118 (2016) 1808–1829, https://doi.org/10.1161/circresaha.116.306923.
[8] T.J. Barrett, et al., Apolipoprotein AI) promotes atherosclerosis regression in diabetic mice by suppressing myelopoiesis and plaque inflammation, Circulation 140 (2019) 1170–1184, https://doi.org/10.1161/circulationaha.119.039476.
[9] T. Hara, et al., Protease-activated receptor-2 plays a critical role in vascular inflammation and atherosclerosis in apolipoprotein E-deficient mice, Circulation 138 (2018) 1706–1719, https://doi.org/10.1161/circulationaha.118.033544.
[10] P.R. Nagareddy, et al., Hyperglycemia promotes myelopoiesis and impairs the resolution of atherosclerosis, Cell Metabol. 17 (2013) 695–708, https://doi.org/10.1016/j.cmet.2013.04.001.
[11] E. Distel, et al., miR 33 inhibition overcomes deleterious effects of diabetes mellitus on atherosclerosis plaque regression in mice, Circ. Res. 115 (2014) 759–769, https://doi.org/10.1161/circresaha.115.304164.
[12] S. Devaraj, et al., Increased monocytic activity and biomarkers of inflammation in patients with type 1 diabetes, Diabetes 55 (2006) 774–779, https://doi.org/10.2337/diabetes.55.03.06.db05-1417.
[13] 2009 E.M. Bradshaw, et al., Monocytes from patients with type 1 diabetes spontaneously secrete proinflammatory cytokines inducing Th17 cells, J. Immunol. 183 (1950) 4432–4439, https://doi.org/10.4049/jimmunol.0900576. Baltimore, Md..
[14] Z. Zhong, et al., New mitochondrial DNA synthesis enables NLRP3 inflammasome activation, Nature 560 (2018) 198–203, https://doi.org/10.1038/s41586-018-0372-z.
[15] J.M. Olefsky, C.K. Glass, Macrophages, inflammation, and insulin resistance, Annu. Rev. Physiol. 72 (2010) 219–246, https://doi.org/10.1146/annurev-physiol-021909-135846.
[16] N. Shanmugam, I.T. Gaw Gonzalo, R. Natarajan, Molecular mechanisms of high glucose-induced cyclooxygenase-2 expression in monocytes, Diabetes 53 (2004) 795–802, https://doi.org/10.2337/diabetes.53.3.795.
[17] D. Vats, et al., Oxidative metabolism and PGC-1 beta attenuate macrophage-mediated inflammation, Cell Metabol. 4 (2006) 13–24, https://doi.org/10.1016/j.cmet.2006.05.011.
[18] J.M. Ellis, et al., Adipose acyl-CoA synthetase-1 directs fatty acids toward beta-oxidation and is required for cold thermogenesis, Cell Metabol. 12 (2010) 53–64, https://doi.org/10.1016/j.cmet.2010.05.012.
[19] J.R. Goldenberg, et al., Preservation of acyl coenzyme A attenuates pathological and metabolic cardiac remodeling through selective lipid trafficking, Circulation 139 (2019) 2765–2777, https://doi.org/10.1161/circulationaha.119.039610.

[20] J.E. Kanter, C. Tang, J.F. Oram, K.E. Bornfeldt, Acyl-CoA synthetase 1 is required for oleate and linoleate mediated inhibition of cholesterol efflux through ATP-binding cassette transporter A1 in macrophages, Biochim. Biophys. Acta 1821 (2012) 358–364, https://doi.org/10.1016/j.bbalip.2011.10.008.

[21] K.E. Bornfeldt, Russell Ross memorial lecture in vascular biology: cellular and molecular mechanisms of diabetes mellitus-accelerated atherosclerosis, Arterioscler. Thromb. Vasc. Biol. 34 (2013) 705–714, https://doi.org/10.1161/atvbaha.113.301928, 2014.

[22] J.E. Kanter, K.E. Bornfeldt, Inflammation and diabetes-accelerated atherosclerosis: myeloid cell mediators, Trends Endocrinol. Metabol.: TEM (Trends Endocrinol. Metab.) 24 (2013) 137–144, https://doi.org/10.1016/j.tem.2012.10.002.

[23] D. Gomez, et al., Interleukin-1β has atheroprotective effects in advanced atherosclerotic lesions of mice, Nat. Med. 24 (2018) 1418–1429, https://doi.org/10.1038/s41591-018-0124-5.

[24] A.C. Finney, et al., EphA2 expression regulates inflammation and fibroproliferative remodeling in atherosclerosis, Circulation 136 (2017) 566–582, https://doi.org/10.1161/circulationaha.116.026644.

[25] R. Wagner, et al., Pathophysiology-based subphenotyping of individuals at elevated risk for type 2 diabetes, Nat. Med. 27 (2021) 49–57, https://doi.org/10.1038/s41591-020-1116-9.

[26] J.Y. Kim, et al., Activating transcription factor 3 is a target molecule linking hepatic steatosis to impaired glucose homeostasis, J. Hepatol. 67 (2017) 349–359, https://doi.org/10.1016/j.jhep.2017.03.023.

[27] M. Wigren, et al., Lack of ability to present antigens on major histocompatibility complex class II molecules aggravates atherosclerosis in ApoE(-/-) mice, Circulation 139 (2019) 2554–2566, https://doi.org/10.1161/circulationaha.118.039288.

[28] M. Westerterp, et al., Cholesterol efflux pathways suppress inflammasome activation, NETosis, and atherogenesis, Circulation 138 (2018) 898–912, https://doi.org/10.1161/circulationaha.117.032636.

[29] L.O. Li, et al., Liver-specific loss of long chain acyl-CoA synthetase-1 decreases triacylglycerol synthesis and beta-oxidation and alters phospholipid fatty acid composition, J. Biol. Chem. 284 (2009) 27816–27826, https://doi.org/10.1074/jbc.M109.022467.

[30] R.A. Coleman, It takes a village: channeling fatty acid metabolism and triacylglycerol formation via protein interactomes, J. Lipid Res. 60 (2019) 490–497, https://doi.org/10.1194/jlr.S091843.

[31] Y. Tang, J. Zhou, S.C. Hooi, Y.M. Jiang, G.D. Lu, Fatty acid activation in carcinogenesis and cancer development: essential roles of long-chain acyl-CoA synthetases, Oncol. Lett. 16 (2018) 1390–1396, https://doi.org/10.3892/ol.2018.8843.

[32] M. Schambelan, et al., Increased prostaglandin production by glomeruli isolated from rats with streptozotocin-induced diabetes mellitus, J. Clin. Invest. 75 (1985) 404–412, https://doi.org/10.1172/jci111714.

[33] P. Xia, R.M. Kramer, G.L. King, Identification of the mechanism for the inhibition of Na+,K(+)-adenosine triphosphatase by hyperglycemia involving activation of protein kinase C and cytosolic phospholipase A2, J. Clin. Invest. 96 (1995) 733–740, https://doi.org/10.1172/jci118117.

[34] A. Yurdagul Jr., et al., Macrophage metabolism of apoptotic cell-derived arginine promotes continual efferocytosis and resolution of injury, Cell Metabol. 31 (2020) 518–533, https://doi.org/10.1016/j.cmet.2020.01.001, e510.

[35] M.M. Gubin, et al., High-dimensional analysis delineates myeloid and lymphoid compartment remodeling during successful immune-checkpoint cancer therapy, Cell 175 (2018) 1014–1030, https://doi.org/10.1016/j.cell.2018.09.030, e1019.

[36] Y. Tang, et al., Research progress on alternative non-classical mechanisms of PCSK9 in atherosclerosis in patients with and without diabetes, Cardiovasc. Diabetol. 19 (2020) 33, https://doi.org/10.1186/s12933-020-01009-4.

[37] M.S. Sabatine, et al., Evolocumab and clinical outcomes in patients with cardiovascular disease, N. Engl. J. Med. 376 (2017) 1713–1722, https://doi.org/10.1056/NEJMoa1615664.

[38] R.S. Rosenson, R.A. Hegele, S. Fazio, C.P. Cannon, The evolving future of PCSK9 inhibitors, J. Am. Coll. Cardiol. 72 (2018) 314–329, https://doi.org/10.1016/j.jacc.2018.04.054.

[39] X. Liu, et al., Inhibition of PCSK9 potentiates immune checkpoint therapy for cancer, Nature 588 (2020) 693–698, https://doi.org/10.1038/s41586-020-2911-7.

[40] A. Sharma, et al., Specific NLRP3 inhibition protects against diabetes-associated atherosclerosis, Diabetes 70 (2021) 772–787, https://doi.org/10.2337/db20-0357.

[41] Intensive diabetes treatment and cardiovascular outcomes in type 1 diabetes: the DCCT/EDIC study 30-year follow-up, Diabetes Care 39 (2016) 686–693, https://doi.org/10.2337/dc15-1990.

[42] D.J. Durgan, et al., Distinct transcriptional regulation of long-chain acyl-CoA synthetase isoforms and cytosolic thioesterase 1 in the rodent heart by fatty acids and insulin, Am. J. Physiol. Heart Circ. Physiol. 290 (2006) H2480–H2497, https://doi.org/10.1152/ajpheart.01344.2005.

[43] M. Rossi Sebastiano, G. Konstantinidou, Targeting long chain acyl-CoA synthetases for cancer therapy, Int. J. Mol. Sci. 20 (2019), https://doi.org/10.3390/ijms20153624.

[44] J.E. Kanter, et al., Diabetes promotes an inflammatory macrophage phenotype and atherosclerosis through acyl-CoA synthetase 1, Proc. Natl. Acad. Sci. U.S.A. 109 (2012) E715–E724, https://doi.org/10.1073/pnas.1111600109.

[45] A. Manichaikul, et al., Genetic association of long-chain acyl-CoA synthetase 1 variants with fasting glucose, diabetes, and subclinical atherosclerosis, J. Lipid Res. 57 (2016) 433–442, https://doi.org/10.1194/jlr.M064592.

[46] F. Al-Rashed, et al., TNF-α induces a pro-inflammatory phenotypic shift in monocytes through ACSL1: relevance to metabolic inflammation, Cell. Physiol. Biochem. : international journal of experimental cellular physiology, biochemistry, and pharmacology 52 (2019) 397–407, https://doi.org/10.33594/000000028.

[47] P.S. Minhas, et al., Restoring metabolism of myeloid cells reverses cognitive decline in ageing, Nature 590 (2021) 122–128, https://doi.org/10.1038/s41586-020-03160-0.

[48] X. Que, et al., Oxidized phospholipids are proinflammatory and proatherogenic in hypercholesterolaemic mice, Nature 558 (2018) 301–306, https://doi.org/10.1038/s41586-018-0198-8.

[49] M. Aouadi, et al., Orally delivered siRNA targeting macrophage Map4k4 suppresses systemic inflammation, Nature 458 (2009) 1180–1184, https://doi.org/10.1038/nature07774.

[50] W. Ying, et al., MiR-690, an exosomal-derived miRNA from M2-polarized macrophages, improves insulin sensitivity in obese mice, Cell Metabol. 33 (2021) 781–790, https://doi.org/10.1016/j.cmet.2020.12.019, e785.

[51] E.P. Stahl, et al., Nonalcoholic fatty liver disease and the heart: JACC state-of-the-art review, J. Am. Coll. Cardiol. 73 (2019) 948–963, https://doi.org/10.1016/j.jacc.2018.11.050.

[52] D.A. Jaitin, et al., Lipid-associated macrophages control metabolic homeostasis in a trem2-dependent manner, Cell 178 (2019) 686–698, https://doi.org/10.1016/j.cell.2019.05.054, e614.

[53] F. Tacke, Targeting hepatic macrophages to treat liver diseases, J. Hepatol. 66 (2017) 1300–1312, https://doi.org/10.1016/j.jhep.2017.02.026.

[54] F.K. Swirski, et al., Identification of splenic reservoir monocytes and their deployment to inflammatory sites, Science (New York, N.Y.) 325 (2009) 612–616, https://doi.org/10.1126/science.1175202.

[55] F. Leuschner, et al., Therapeutic siRNA silencing in inflammatory monocytes in mice, Nat. Biotechnol. 29 (2011) 1005–1010, https://doi.org/10.1038/nbt.1989.

[56] P. Dutta, et al., Myocardial infarction accelerates atherosclerosis, Nature 487 (2012) 325–329, https://doi.org/10.1038/nature11260.

[57] J.L. Witztum, Splenic immunity and atherosclerosis: a glimpse into a novel paradigm? J. Clin. Invest. 109 (2002) 721–724, https://doi.org/10.1172/jci15310.

[58] X.M. Ai, et al., The role of splenectomy in lipid metabolism and atherosclerosis (AS), Lipids Health Dis. 17 (2018) 186, https://doi.org/10.1186/s12944-018-0841-2.

[59] D. Karunakaran, et al., RIPK1 expression associates with inflammation in early atherosclerosis in humans and can Be therapeutically silenced to reduce NF-κB activation and atherogenesis in mice, Circulation 143 (2021) 163–177, https://doi.org/10.1161/circulationaha.118.038379.

[60] S. Jeon, et al., Anti-inflammatory actions of soluble ninjurin-1 ameliorate atherosclerosis, Circulation 142 (2020) 1736–1751, https://doi.org/10.1161/circulationaha.120.046907.

[61] K.J. Moore, I. Tabas, Macrophages in the pathogenesis of atherosclerosis, Cell 145 (2011) 341–355, https://doi.org/10.1016/j.cell.2011.04.005.

[62] G.J. Koelwyn, E.M. Corr, E. Erbay, K.J. Moore, Regulation of macrophage immunometabolism in atherosclerosis, Nat. Immunol. 19 (2018) 526–537, https://doi.org/10.1038/s41590-018-0113-3.

[63] P.A. Mueller, et al., Deletion of macrophage low-density lipoprotein receptor-related protein 1 (LRP1) accelerates atherosclerosis regression and increases C-C chemokine receptor type 7 (CCR7) expression in plaque macrophages, Circulation 138 (2018) 1850–1863, https://doi.org/10.1161/circulationaha.117.031702.

[64] X. Hou, et al., Vitamin lipid nanoparticles enable adoptive macrophage transfer for the treatment of multidrug-resistant bacterial sepsis, Nat. Nanotechnol. 15 (2020) 41–46, https://doi.org/10.1038/s41565-019-0600-1.

[65] P.F. Ma, et al., Cytotherapy with M1-polarized macrophages ameliorates liver fibrosis by modulating immune microenvironment in mice, J. Hepatol. 67 (2017) 770–779, https://doi.org/10.1016/j.jhep.2017.05.022.

[66] T. Hagemann, et al., Re-educating" tumor-associated macrophages by targeting NF-kappaB, J. Exp. Med. 205 (2008) 1261–1268, https://doi.org/10.1084/jem.20080108.

[67] S.M. Pyonteck, et al., CSF-1R inhibition alters macrophage polarization and blocks glioma progression, Nat. Med. 19 (2013) 1264–1272, https://doi.org/10.1038/nm.3337.

[68] S. Lee, S. Kivimäe, A. Dolor, F.C. Szoka, Macrophage-based cell therapies: the long and winding road, J. Contr. Release : official journal of the Controlled Release Society 240 (2016) 527–540, https://doi.org/10.1016/j.jconrel.2016.07.018.

[69] R. Andreesen, et al., Adoptive transfer of tumor cytotoxic macrophages generated in vitro from circulating blood monocytes: a new approach to cancer immunotherapy, Cancer Res. 50 (1990) 7450–7456.

[70] F. Moroni, et al., Safety profile of autologous macrophage therapy for liver cirrhosis, Nat. Med. 25 (2019) 1560–1565, https://doi.org/10.1038/s41591-019-0599-8.

[71] S.J. Jenkins, et al., Local macrophage proliferation, rather than recruitment from the blood, is a signature of TH2 inflammation, Science (New York, N.Y.) 332 (2011) 1284–1288, https://doi.org/10.1126/science.1204351.